

Adaptive Conformal Prediction Intervals Over Trajectory Ensembles

Ruipu Li¹, Daniel Menacho^{1,2}, Alexander Rodríguez¹

¹ University of Michigan, ² Pontifical Catholic University of Peru
 {liruipu, dmenordo, alrodri}@umich.edu

Abstract

Future trajectories play an important role across domains such as autonomous driving, hurricane forecasting, and epidemic modeling, where practitioners commonly generate ensemble paths by sampling probabilistic models or leveraging multiple autoregressive predictors. While these trajectories reflect inherent uncertainty, they are typically uncalibrated. We propose a unified framework based on conformal prediction that transforms sampled trajectories into calibrated prediction intervals with theoretical coverage guarantees. By introducing a novel online update step and an optimization step that captures inter-step dependencies, our method can produce discontinuous prediction intervals around each trajectory, naturally capture temporal dependencies, and yield sharper, more adaptive uncertainty estimates.

Code — <https://github.com/complex-ai-lab/cp-traj>

Introduction

In multi-step time series forecasting, probabilistic forecasting methods are becoming increasingly popular. Driven by recent advances in generative models, various architectures have been designed for time series forecasting, including those based on generative adversarial networks (GANs) (Yoon, Jarrett, and Van der Schaar 2019; Vuletić, Prenzel, and Cucuringu 2024), diffusion models (Shen and Kwok 2023; Feng et al. 2024) and normalizing flows (Yalavarthi et al. 2025). As illustrated in Figure 1, these methods provide the conditional distribution of future outcomes, enabling the sampling of multiple possible trajectories that represent diverse plausible scenarios—each of which can inform planning decisions. However, while sampled trajectories capture predictive variability, they are typically uncalibrated in their uncertainty quantification (UQ)—that is, the probabilities implied by the spread of samples do not align with empirical outcome. This lack of calibration arises from imperfections in the learned conditional distribution, potentially stemming from model misspecification, limited data, or other sources of bias.

In this paper, we focus on UQ for trajectory samples (or ensembles) in an online setting, where time series data arrive sequentially and both predictions and their associated uncertainties must be continuously updated as new information becomes available. This problem setting is critical for

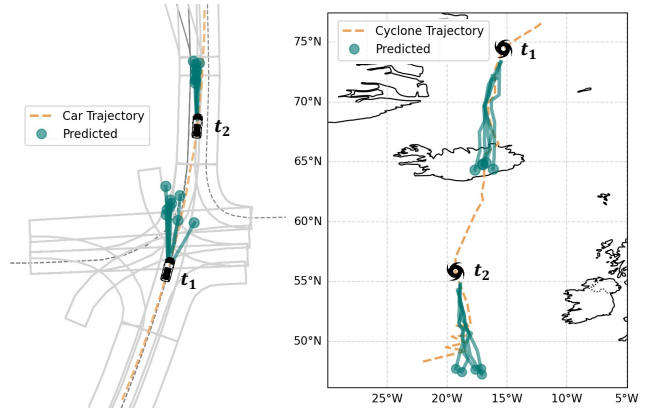


Figure 1: Examples of trajectory ensembles. **Left:** In autonomous driving, algorithms generate multiple future trajectories of nearby vehicles to anticipate maneuvers such as turning, lane changes, or continuing straight—critical for safe navigation. **Right:** In cyclone forecasting, algorithms predict possible future paths to inform preparedness and response efforts. In both cases, two prediction steps are shown (t_1 and t_2). The orange dashed line represents the ground truth trajectory, while the green trajectories denote sampled predictions from a generative model.

many real-world applications, including autonomous driving, weather forecasting, and epidemic prediction (Chang et al. 2019; Ullrich and Zarzycki 2017; Rodríguez et al. 2024). The online setting demands UQ methods that can adapt in real-time and maintain valid coverage guarantees as the data distribution evolves. Online conformal prediction (OCP) methods (Gibbs and Candes 2021; Angelopoulos, Candes, and Tibshirani 2023) address this by ensuring: (1) *Adaptivity*: intervals adjust to temporal distribution shifts; (2) *Validity*: long-term coverage converges to the user-specified rate; and (3) *Efficiency*: intervals are as narrow as possible once validity and adaptivity are achieved. However, UQ for sampled trajectories introduces unique challenges, motivating several key considerations for designing effective UQ methods. (i) *Diverging trajectories*: Trajectories can be highly diverse and diverge over time, as illustrated in Figure 1, leading to multimodal and/or disjoint

trajectory distributions. We propose to account for diverging paths and construct prediction intervals using them as a backbone. (ii) *Inter-step dependencies*: Reliable decision-making may require coverage across multiple forecast steps, i.e., multi-step calibration (Lim et al. 2021). To achieve this, we propose connecting forecast horizons and leveraging their inter-step dependencies, which is also essential for constructing sharper prediction intervals. (iii) *Auxiliary information*: We propose leveraging domain-specific auxiliary information to enhance calibration. For example, it is desirable to model the progressive increase in uncertainty over time, as observed in complex dynamical systems like weather prediction (Ouyang and Yin 2018; Cachay et al. 2025), and in influenza forecasting (Kamarthi et al. 2021).

Why Existing Conformal Prediction (CP) Methods Fail in Our Problem Setting?

First, prior conformal prediction methods for generative models assume exchangeability and lack the flexibility to handle structured samples, such as trajectories, where each sample consists of multiple correlated predictions that must be treated individually. Recent advances in this space include Probabilistic Conformal Prediction (PCP) (Wang et al. 2023), a novel non-conformity score based on samples drawn from an arbitrary conditional generative model and constructs prediction regions by placing circles with a calibrated radius around each sample. PCP-CRC (Zecchin, Park, and Simeone 2024) further extends the non-conformity score from PCP to multi-step time series forecasting. However, both procedures assume exchangeability and operate offline; therefore, they cannot readily work with evolving data streams. Furthermore, because PCP-CRC calibrates a single non-conformity score across all forecast horizons, it denies users the ability to tighten or loosen uncertainty at specific lead times adaptively based on coverage conditions. Second, achieving accurate coverage across multiple forecast steps and incorporating auxiliary information often conflict with the design of current online CP methods. As noted above, a key requirement for these methods is to maintain a long-term coverage guarantee. Typically, this guarantee is achieved using online gradient descent on the quantile loss (Gibbs and Candes 2021; Angelopoulos, Candes, and Tibshirani 2023). However, this leaves little flexibility for further adaptation, making it impossible to adjust based on coverage across forecast steps or leverage available context to enhance predictive performance.

Our Contributions

To address the aforementioned challenges, we propose CP-Traj, a novel approach designed to build prediction intervals around sampled trajectories, thereby fully leveraging the rich information from conditional distributions. Our key contributions are as follows:

1. We present CP-Traj, a novel framework for multi-step online conformal prediction that calibrates prediction intervals directly around sampled trajectories. Unlike prior methods, CP-Traj is designed to accommodate both the potential divergence of trajectories and the inter-step dependencies that naturally arise in the setting.

2. CP-Traj provides long-term coverage guarantees for each forecast step. We employ a novel online update step, which enables an additional optimization process that explicitly connects prediction intervals across the entire forecast horizon, thereby improving the coverage and efficiency by capturing inter-step correlations.
3. Comprehensive experiments on a wide range of synthetic and real-world datasets show that CP-Traj achieves consistently better coverage and tighter intervals than state-of-the-art baselines, underscoring the benefits of the proposed method.

Problem Setup

In this section, we formally define the problem and introduce the necessary notation.

Let $x_t \in \mathbb{R}^N$ denote the observed features at time step t , where N is the feature dimension. The target variable at time t is $y_t \in \mathbb{R}$ (for simplicity, assumed to be scalar; extension to vectors is straightforward). For each forecast step $h \in [1, H]$, we denote the prediction target h steps ahead of time t as $y_t^h := y_{t+h}$, representing the true outcome at time $t+h$ to be predicted based on information available at time t . For sequences, we use the shorthand $x_{t_1:t_2} := (x_{t_1}, \dots, x_{t_2})$, and similarly for y . Assume we have access to a probabilistic forecasting model f that, given past observations $x_{1:t}$, outputs a predictive distribution over future target values: $f(x_{1:t}) = \hat{p}(\hat{y}_t^1, \dots, \hat{y}_t^H \mid x_{1:t})$, where H denotes the forecast horizon, and $\hat{y}_t^1, \dots, \hat{y}_t^H$ are the model’s predicted values for each of the next H time steps. A single sampled trajectory from this predictive distribution is denoted as $\hat{y}_t^{(m)} := (\hat{y}_t^{1,(m)}, \dots, \hat{y}_t^{H,(m)})$, where $\hat{y}_t^{(m)} \sim \hat{p}(\hat{y}_t^1, \dots, \hat{y}_t^H \mid x_{1:t})$, and m indexes the sample. Given a user-specified coverage rate $1 - \alpha$, our goal is to construct a collection of prediction intervals for each forecast step at time t , denoted as $C_t^{1:H} := [C_t^1, \dots, C_t^H]$. In multi-step time series forecasting, calibration performance can be considered along two dimensions: over time steps t and across forecast horizons h :

Obj. 1 (coverage across time steps t): Our first goal is constructing $C_t^{1:H}$ so that:

$$\min \left| \frac{1}{T} \sum_{t=1}^T \mathbf{1}(y_t^h \notin C_t^h) - \alpha \right| + \frac{1}{T} \sum_{t=1}^T |C_t^h|, \forall h \in [1, H] \quad (1)$$

where $\mathbf{1}(\cdot)$ denotes the indicator function. Equation 1 requires that the coverage error (miscoverage) rate converges to the user-specified miscoverage rate α , while keeping the prediction intervals as tight as possible. This convergence is known as *long-term coverage* (Gibbs and Candes 2021).

Obj. 2 (coverage across forecast horizons h): A common objective in multi-step time series forecasting is *marginal coverage* across the forecast horizon at each time step (Lim et al. 2021), which can be expressed as:

$$\min \left| \frac{1}{H} \sum_{h=1}^H \mathbf{1}(y_t^h \notin C_t^h) - \alpha \right|, \forall t \in [1, T] \quad (2)$$

where the goal is to minimize the gap between the empirical marginal miscoverage (averaged across all H steps at time t) and the desired miscoverage rate α .

Obj. 3 (user-specified multi-step objective) We propose a generalization of Objective 2 to account for scenarios where further optimization across the forecast horizon is required or desirable. This can be formalized as:

$$\min J(C_t^{1:H}), \quad (3)$$

where J is a user-defined objective function that measures the quality of the prediction intervals $C_t^{1:H}$. This objective function can help us incorporate the auxiliary information previously discussed. We will provide specific examples of J in our experiments section.

Remark: It is important to emphasize that, while Obj. 1 and Obj. 2 are not new, previous work has only studied them separately. Obj. 1 has been the main focus of work on OCP (Gibbs and Candes 2021; Angelopoulos, Candes, and Tibshirani 2023; Gibbs and Candès 2024; Li and Rodríguez 2025). Obj. 2 has been a focus in multi-step probabilistic forecasting (Lim et al. 2021). A similar objective has been employed in OCP by BCI (Yang, Candès, and Lei 2024), which leverages Obj. 2 within a model predictive control framework to improve performance on Obj. 1. It is worth noting that BCI still addresses one-step ahead forecasting. Obj. 3 is a novel generalization introduced in this paper.

Method

Our method is motivated by the observation that existing online conformal prediction (OCP) methods cannot be effectively used in trajectory samples as they lack the flexibility to coordinate adaptation across forecast horizons. Most current OCP methods adjust prediction intervals for each forecast horizon independently (Obj. 1). However, this independent treatment may result in inconsistencies across horizons and does not allow us to incorporate multi-step objectives (Obj. 2 & 3). Inspired by recent work in model predictive control (MPC) for conformal prediction (Yang, Candès, and Lei 2024), we propose to integrate an optimization step across the forecast horizon to address this limitation. This enables calibration thresholds α to be adapted in anticipation of coverage violations in future forecast steps. However, standard online updates in OCP methods typically produce a single value at each step—leaving no flexibility for horizon-wide optimization. To address this, we introduce a modified online update that produces a set of candidate values, each of which guarantees long-term coverage (Obj. 1). These candidate values are then passed to an MPC step, which selects the final calibration threshold by optimizing expected future performance across the entire horizon (Obj. 2 & 3).

In this section, we first describe how to adapt OCP methods to the setup of multi-step time series forecasting with generative models. Next, we present our novel online update step, which generates a set of candidate values and provides a proof of validity, demonstrating that our approach maintains long-term coverage guarantees. Finally, we detail the optimization step that selects the final calibration threshold based on these candidate values.

OCP for Sampled Trajectories

Multi-step forecasting with ACI: The adaptive conformal inference (ACI) algorithm proposed by (Gibbs and Candes 2021) is one of the earliest and most influential works in online conformal prediction. Instead of using a fixed calibration threshold α , ACI introduces a time-varying threshold α_t , which is updated at each time step according to the observed coverage error: $\alpha_{t+1} = \alpha_t - \gamma(\text{err}_t - \alpha)$, where γ is the step size and $\text{err}_t = \mathbf{1}(y_t \notin C_t)$ indicates a coverage violation at time t . The prediction interval is then constructed as $C_t = \{y : s_t(\hat{y}_t, y) \leq \text{Quantile}_{1-\alpha_t}(S_t)\}$, where s_t is the non-conformity score function and S_t is the set of past scores. This update enables ACI to maintain long-term coverage even under non-stationary conditions.

Although ACI is designed for one-step ahead forecasting, it can be easily extended to construct prediction intervals for multi-step forecasting by maintaining separate α_t^h for each forecast horizon. At each time step, the procedure updates α_t^h separately for each horizon based on the observed coverage errors. However, as discussed earlier, this approach treats the prediction intervals for each horizon independently and does not allow adaptation based on the coverage conditions of other horizons. As a result, it may fail to capture potential dependencies across horizons within the forecast trajectory. Similar limitations arise when other popular online conformal prediction methods are adapted to the multi-step setting (Angelopoulos, Candes, and Tibshirani 2023; Gibbs and Candès 2024; Yang, Candès, and Lei 2024; Li and Rodríguez 2025).

Non-conformity Score for Samples The development of generative models has underscored the need for effective methods to quantify the uncertainty associated with generated samples. The PCP score, proposed by (Wang et al. 2023), is specifically designed to address this need. PCP defines a non-conformity score for a set of samples as the minimum distance between the observation and the generated samples, enabling the construction of prediction regions around each sample. More formally, given a set of samples $\hat{\mathcal{Y}} = \{\hat{y}^{(m)} \mid m \in [1, M]\}$ and an observation y , the non-conformity score is defined as

$$s_t(y, \hat{\mathcal{Y}}) = \min_{\hat{y} \in \hat{\mathcal{Y}}} \|y - \hat{y}\|.$$

Given a set of non-conformity scores S , the calibration radius is $r = \text{Quantile}_{1-\alpha}(S)$, and the prediction region is constructed as $C = \bigcup_{m=1}^M \{y \mid \|y - \hat{y}^{(m)}\| \leq r\}$. Note that the coverage guarantee of this score relies on the assumption that the samples are i.i.d., a condition that is satisfied for trajectories generated by generative models. Under this assumption, the approach can also be extended to multi-step predictions produced by ensembles of models.

We adopt the PCP score because it naturally captures the structure and diversity of the generated samples. In contrast to traditional non-conformity scores such as the absolute residual—which rely on a single point estimate (e.g., the mean or median of the samples)—the PCP score utilizes the entire set of generated trajectories. This enables it to account for the multimodal and correlated nature of the predictive distribution. Consequently, the PCP score produces

prediction intervals that more accurately reflect the underlying uncertainty and dependencies in the data, resulting in improved calibration and sharper intervals, as demonstrated in our experimental results.

Online Update

As shown in the previous section, the standard ACI procedure produces a fixed calibration threshold α_t at each time step t , leaving no room for further optimization. We propose an extended version of ACI that, instead of a single value, outputs a set $I_t = [\alpha_t - \delta_t, \alpha_t + \delta_t]$ at each time step, where $\delta_t = o(t)$ defines the radius of the prediction interval. By selecting an appropriate radius δ_t , the long-term coverage guarantee is still maintained for any $\alpha \in I_t$ (see Theorem 1). The proof is given in the Appendix. Our novel online update leaves us room for optimizing for Obj. 2 & Obj. 3 while still guaranteeing long-term coverage (Obj. 1). The detailed update step is shown in Algorithm 1. At each time step, we first generate predictions in the form of a set of samples. For each horizon h , if the ground truth is observed (i.e., $t - h > 0$), we compute the non-conformity score and add it to the corresponding set of non-conformity scores. The calibration threshold α is then updated based on the observed coverage condition. Subsequently, we obtain a range I_t^h for each horizon, where in our experiments we set $\delta_t = \frac{D}{\sqrt{t}}$, with D as a constant. We then solve for $\alpha^{1*}, \dots, \alpha^{H*}$ by optimizing the objective function J , and use these calibration thresholds to construct the final prediction intervals.

Theorem 1. *For any horizon h , when $\delta_t = o(t)$, applying the update step in Algorithm 1 produces a range of calibration threshold values I_t^h at each time step t . For any $\alpha^{h*} \in I_t^h$, the procedure guarantees long-term coverage.*

Optimization

As shown above, the novel online update design constructs H sets of values I_t^h for $h \in [1, H]$, allowing for flexible selection at each horizon based on inter-step dependencies. Our optimization step leverages this flexibility, enabling the calibration thresholds to be jointly optimized across the forecast horizon, which connects the coverage conditions across different horizons, resulting in prediction intervals that are more adaptive to distributional changes and better tailored to user requirements. When there are no specific user requirements, we use the objective function given in Equation 2 (which optimizes coverage across the forecast horizon), allowing us to leverage the inter-step dependencies. From the perspective of model predictive control, this objective guides the selection of calibration thresholds based on possible future outcomes, thereby improving overall calibration performance. The optimization step is adapted from Bellman conformal inference (Yang, Candès, and Lei 2024), which formulates calibration threshold selection as a stochastic control problem and uses dynamic programming to jointly optimize interval length and coverage over a receding horizon. In the following section, we use this objective function as an example to show how the optimization step works.

Remark: As long as the calibration threshold remains

Algorithm 1: Online Conformal Prediction with Horizon-Wide Calibration

Input: Generative model f , user-specified miscoverage rate α , objective function J , total number of forecast horizons H , trajectory sample size M , learning rate η

Initialization: For each horizon $h \in [1, H]$, set $\alpha_0^h = \alpha$ and initialize a set $S^h = \{\infty\}$ for non-conformity scores.

Output: Calibrated prediction intervals $C_t^{1:H}$ for each t .

```

1: for  $t = 1, \dots, T$  do
2:   Observe most recent features  $x_t$  and target value  $y_t$ 
3:   Generate  $M$  sampled trajectories, i.e., for  $m = 1, \dots, M$ , sample  $\hat{y}_t^{(m)} \sim f(x_{1:t})$ .
4:   For each horizon  $h$ , set  $\hat{\mathcal{Y}}_t^h := \cup_{m=1}^M \hat{y}_t^{h(m)}$ .
5:   for  $h = 1, \dots, H$  do
6:     if  $t' = t - h > 0$  then
7:       Compute score:  $s_{t'}^h := s_t(y_t, \hat{\mathcal{Y}}_t^h)$ 
8:       Update set:  $S^h \leftarrow S^h \cup \{s_{t'}^h\}$ 
9:       Compute coverage error:  $\text{err}_{t'}^h = \mathbf{1}(y_t \notin C_{t'}^h)$ 
10:      Update:  $\alpha_{t'}^h = \alpha_{t'-1}^h - \eta(\text{err}_{t'}^h - \alpha)$ 
11:    else
12:      Update:  $\alpha_{t'}^h = \alpha_{t'-1}^h$ 
13:    end if
14:  end for
15:  For each  $h$ , obtain  $I_t^h = [\alpha_{t'}^h - \delta_t, \alpha_{t'}^h + \delta_t]$ 
16:  Solve for horizon-wide calibration thresholds by optimizing  $J$ :

```

$$(\alpha^{1*}, \dots, \alpha^{H*}) = \underset{u_1 \in I_t^1, \dots, u_H \in I_t^H}{\operatorname{argmin}} J(C_t^{1:H})$$

```

17:  for  $h = 1, \dots, H$  do
18:    Construct calibrated prediction interval:  $C_t^h = \{y \mid$ 
19:       $s_t(y, \hat{\mathcal{Y}}_t^h) \leq \text{Quantile}_{1-\alpha^{h*}}(S^h)\}$ 
20:  end for

```

within the range determined by the update step, the optimization step can take any form that best suits the user's practical needs.

The optimization problem is formulated as follows:

$$\min_{u_1 \in I_t^1, \dots, u_H \in I_t^H} J_1 + \lambda J_2 \quad (4)$$

where

$$J_1 = \max \left\{ \frac{1}{H} \sum_{h=1}^H \mathbf{1}(y_t^h \notin C_t^h) - \alpha, 0 \right\} \quad (5)$$

$$J_2 = \frac{1}{H} \sum_{h=1}^H \|C_t^h\| \quad (6)$$

Here, the control actions u_h , $h \in [1, H]$ are possible values of the calibration thresholds. J_1 penalizes large coverage gaps across the horizon, ensuring that the empirical miscoverage does not exceed the target. J_2 measures the average width (or size) of the prediction intervals across all horizons, promoting efficiency. The trade-off between coverage

and efficiency is controlled by the parameter λ , which is typically set to a small value to prioritize coverage.

Approximation of y_t : Since the ground truth values $y_t^{1:H}$ (i.e., $y_{t+1:t+H}$) are not observed at time t , we must approximate them for optimization. Let the prediction interval associated with a calibration threshold β be defined as

$$C_t^h(\beta) := \left\{ y \mid s_t(y, \hat{y}_t^h) \leq \text{Quantile}_{1-\beta}(S^h) \right\}.$$

For each observed ground truth value in the past, we can compute the optimal calibration threshold β_t^h as

$$\beta_t^h := \sup \left\{ \beta \mid y_t^h \in C_t^h(\beta) \right\},$$

which represents the largest β (smallest prediction interval) such that the ground truth is still covered by the interval. Define the empirical distribution $F_t^h := \{\beta_{t-h}^h, \dots, \beta_{t-B}^h\}$, which is the collection of optimal thresholds from the past B instances for horizon h . We then sample $\beta_t^h \sim F_t^h$ and use this as a surrogate for the unobserved ground truth at time t . In the optimization, a miscoverage occurs whenever the chosen calibration threshold u_h is larger than β_t^h , i.e., $\text{err}_t^h = \mathbf{1}(u_h > \beta_t^h)$. Define the cumulative number of errors up to horizon h as $\rho^h = \sum_{k=1}^h \text{err}_t^k$. The optimization problem described in Equation 4 can now be rewritten in terms of β and ρ as:

$$\min_{u_1 \in I_t^1, \dots, u_H \in I_t^H} \mathbb{E}_{\beta_t^h \sim F_t^h, h \in [1, H]} [J_1 + \lambda J_2] \quad (7)$$

$$J_1 = \max \left\{ \frac{\rho^H}{H} - \alpha, 0 \right\}, J_2 = \sum_{h=1}^H (1 - \hat{\beta}^h). \quad (8)$$

Adaptivity: In real-world applications, the distribution of the true β_t^h often differs from the empirical distribution F_t^h due to potential distribution shifts. This discrepancy can degrade the performance of the optimization. To address this, we incorporate an adaptation mechanism for the target horizon coverage α based on past coverage errors. Specifically, the target coverage is updated as follows:

$$\alpha_{t+1} = \alpha_t - \eta \left(\frac{1}{H} \sum_{h=1}^H \mathbf{1}(y_t^h \notin C_t^h) - \alpha \right),$$

where η is the adaptation step size. Accordingly, the objective term J_1 becomes

$$J_1 = \max \left\{ \frac{\rho^H}{H} - \alpha_t, 0 \right\}.$$

This adaptation mechanism allows the target coverage level to be dynamically updated based on recent empirical coverage, making the method more robust to distributional changes and improving calibration performance in non-stationary environments.

Experiments

Experimental Setting

Datasets and Base Forecasters. We evaluate our approach on three real-world datasets—autonomous navigation (*Lane*), climate forecasting (*Cyclone*), and healthcare

(*Flusight*)—as well as a synthetic dataset (*Markovar*). The **Lane** dataset is based on an autonomous vehicle dataset from Argoverse (Chang et al. 2019) and contains 250 sequences with a 5-step prediction horizon. The **Cyclone** dataset is based on data from Weather Lab¹ (Ullrich and Zarzycki 2017; Zarzycki and Ullrich 2017; Ullrich et al. 2021), a platform providing forecasts for cyclone. We use 30 historical cyclone scenarios, each lasting at least 4 days, with 5 predicted trajectories over an 8-step horizon. The **Markovar** dataset is synthetically generated using a Markovian Auto-Regressive (MarkovAR) process. At each step, 16 predicted trajectories are generated over a 32-step horizon. We simulate three sequences of 500 observations each. The **Flusight** dataset is constructed from CDC FluSight records² (Mathis et al. 2024), which include weekly influenza hospitalization data. We use 50 sequences from distinct U.S. locations (excluding those with insufficient data), with each sequence spanning about 50 weeks during the 2023-2024 and 2024-2025 flu seasons and containing 5 trajectories over a 4-step horizon.

Baselines. We compare CP-Traj with four popular online conformal prediction methods: (i) *ACI* (Gibbs and Candès 2021), which adapts the calibration threshold α_t over time to achieve valid long-term coverage; (ii) *NEXCP* (Barber et al. 2023), which adjusts non-conformity score weights to handle distribution shifts; (iii) *FACI* (Gibbs and Candès 2024), which aggregates multiple learning rates for improved adaptivity without manual tuning; and (iv) *SAOCP* (Bhatnagar et al. 2023), which combines predictors over multiple timescales to enhance calibration under dynamic conditions.

Evaluation Metrics. The methods are evaluated in terms of probabilistic accuracy, calibration, and efficiency using metrics that are widely adopted in the literature (Li and Rodríguez 2025). The primary metrics considered are the calibration score (CS), which evaluates probabilistic accuracy and calibration, and the interval width, which assesses efficiency. The CS is defined as the average difference between the target coverage and the empirical coverage across a range of miscoverage rates. For one-dimensional data, the interval width is the length between the upper and lower bounds. For two-dimensional data, the interval width corresponds to the area covered by the prediction sets.

For each dataset, we report the mean value of each metric across multiple sequences, with error bars indicating standard deviations. Additional details on the experimental setup and datasets are provided in the Appendix.

Main Results

In our experiments, each method is evaluated across eleven miscoverage rates: 0.02, 0.05, 0.1, 0.2, 0.3, 0.4, 0.5, 0.6, 0.7, 0.8, and 0.9, providing a comprehensive assessment at different coverage levels. More emphasis is placed on higher coverage rates (i.e., smaller miscoverage rates), as these are of greater practical importance (Cramer et al. 2022).

Comparison on Overall Performance. Table 1 presents the main results. The calibration score is averaged across all se-

¹<https://deepmind.google.com/science/weatherlab>

²<https://github.com/cdcepi/FluSight-forecast-hub>

Table 1: Calibration score (CS) and interval width (Width) for five methods on four datasets. The best scores are highlighted in **bold**, and the second best are underlined. Interval widths are averaged across all miscoverage rates. CP-Traj achieves the best calibration score on all datasets and is competitive in terms of interval width.

Dataset	Metric	CP-Traj	ACI	NeXCP	FACI	SAOCP
Cyclone	CS	0.064 ± 0.030	0.133 ± 0.041	<u>0.088</u> ± 0.039	0.117 ± 0.043	0.100 ± 0.017
	Width	1.777 ± 0.442	1.219 ± 0.311	5.399 ± 0.480	6.301 ± 0.562	<u>1.581</u> ± 0.582
Lane	CS	0.099 ± 0.059	0.168 ± 0.080	<u>0.124</u> ± 0.057	0.138 ± 0.062	0.187 ± 0.046
	Width	<u>1.752</u> ± 0.579	1.005 ± 0.388	6.954 ± 1.654	6.981 ± 1.302	9.824 ± 2.653
FluSight	CS	0.037 ± 0.006	0.073 ± 0.009	0.075 ± 0.020	<u>0.072</u> ± 0.021	0.356 ± 0.032
	Width	2838 ± 2254	3824 ± 1789	798 ± 2621	<u>802</u> ± 2598	6201 ± 2632
MarkovAR	CS	0.027 ± 0.002	0.044 ± 0.002	0.049 ± 0.002	<u>0.038</u> ± 0.009	0.206 ± 0.012
	Width	<u>2.426</u> ± 0.085	1.781 ± 0.095	2.754 ± 0.023	3.015 ± 0.084	2.708 ± 0.122

Table 2: Comparison of calibration score (CS) and interval width between CP-Traj and CP-Traj (w/ RS), which uses the absolute residue score. The results show that using the PCP score consistently provides better coverage and generally improves efficiency.

Method	Cyclone		Lane		Flusight		Markovar	
	CS	Width	CS	Width	CS	Width	CS	Width
CP-Traj	0.064	1.777	0.099	1.752	0.036	18025.589	0.028	2.306
CP-Traj (w/ RS)	0.095	2.121	0.101	2.096	0.041	16695.386	0.035	4.625

quences for each dataset. The interval width reported is the average over all miscoverage rates, all forecast steps and all sequences, consistent with the computation of the calibration score. The results demonstrate that CP-Traj consistently achieves superior calibration scores with good efficiency on all evaluated datasets. While NEXCP and FACI generally perform well in terms of calibration score, their efficiency, as measured by interval width, is consistently worse than CP-Traj on all datasets except Flusight. Notably, for Cyclone and Lane, the interval widths for NEXCP and FACI are more than two times and three times larger than ours, respectively. These results demonstrate the superior calibration performance of CP-Traj and show that, by accounting for inter-step dependency, our method is able to achieve both sharper and more effective prediction intervals.

It is worth noting that, in all cases, we adopt the same experimental settings as ACI. As noted earlier, the main difference between CP-Traj and ACI is that we extend the calibration threshold to a set of values and solve for the best value by optimizing for multi-step coverage at each time step. This modification leads to a substantial improvement in calibration score compared to ACI across all four datasets, demonstrating the effectiveness of the optimization step.

Analysis of 90% Prediction Interval Performance Across Horizons on Cyclone. To gain a deeper understanding of the performance, we present the coverage rate and interval width of the 90% prediction interval ($\alpha = 0.1$) for each forecast horizon on the Cyclone dataset, as shown in Figure 2. The target 90% coverage rate is indicated by a dashed black line for reference; the closer a method’s curve is to this line, the better its empirical coverage. From the figure, it is clear that the coverage of CP-Traj remains consistently

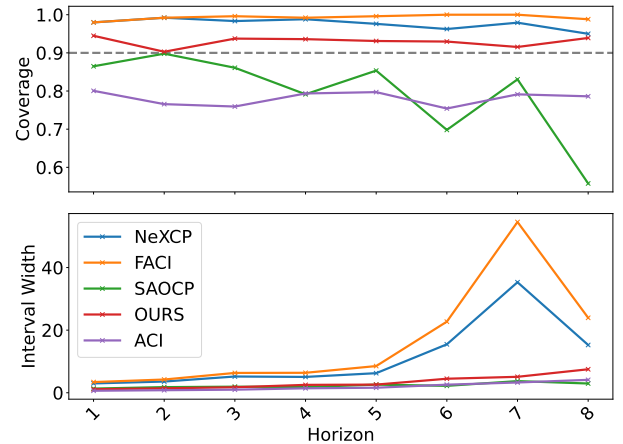


Figure 2: Coverage rate and interval width of 90% prediction intervals for each forecast horizon on the Cyclone dataset. The dashed black line indicates the target 90% coverage. CP-Traj consistently maintains accurate coverage close to the target while producing sharper intervals than baselines. Results are averaged over all sequences.

closer to the reference line for all horizons. In contrast, ACI and SAOCP both tend to undercover, with coverage curves lying below the reference, while NEXCP and FACI always overcover, producing overly wide prediction intervals. These results demonstrate that CP-Traj achieves the sharpest prediction intervals with valid coverage across all horizons.

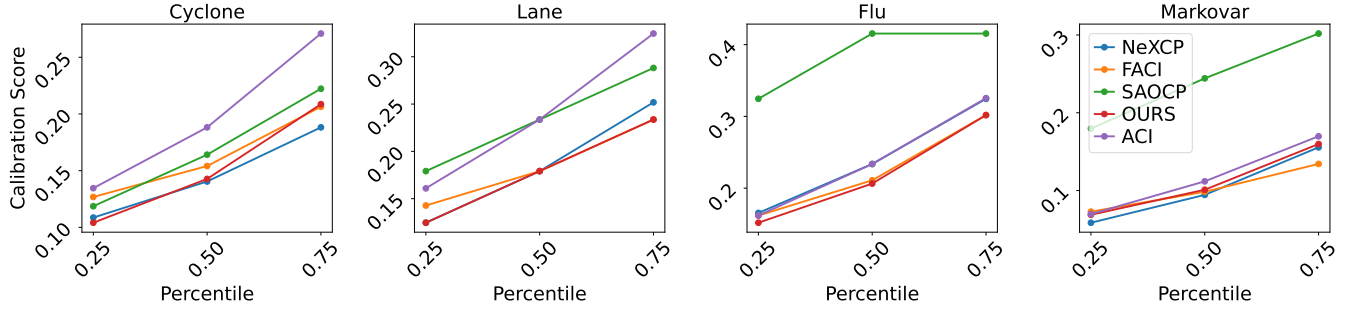


Figure 3: Comparison of horizon coverage measured by calibration score. For each method, we compute the calibration score across the forecast horizon for each time step, and then show the 0.25, 0.5, and 0.75 percentiles of these calibration scores. Our method is shown in red. CP-Traj achieves the best or close to the best performance in most cases.

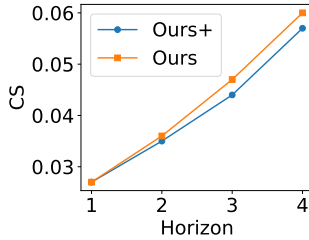


Figure 4: Comparison of CP-Traj with (Ours+) and without (Ours) an auxiliary objective that encourages interval width to increase with horizon.

Does Horizon-Wide Optimization Improve the Objective? The flexibility of CP-Traj allows calibration thresholds to be selected from a range of values by optimizing an objective function defined across the prediction horizon. Using horizon coverage (Obj. 2) as the optimization objective has been proven to be effective in improving overall calibration performance (i.e., achieving better Obj. 1), as shown in Table 1 and Figure 2. In Figure 3, we show that horizon coverage is indeed improved through the optimization step. We average the coverage across horizons at every time step to obtain the horizon coverage, whose calibration score is calculated across all miscoverage rates, and the 0.25, 0.5, and 0.75 percentiles of these scores are reported in Figure 3. Compared to ACI, which does not include the optimization step, CP-Traj consistently achieves lower calibration scores, proving improved horizon coverage. Among all methods, CP-Traj is best or close to best in most cases. It is worth noting that NEXCP attains very competitive calibration on Cyclone, Lane, and Markovar; however, as shown in Table 1, this comes at the cost of significantly reduced efficiency.

Incorporating Auxiliary Information via an Additional Objective. Uncertainty in multi-step time series forecasting typically increases with forecast horizon. To capture this, we add an objective that favors wider intervals at larger horizons and evaluate it on the Flusight dataset (see details in Appendix). Figure 4 shows the calibration score per horizon for CP-Traj with and without this term, with shaded bands indicating one standard deviation across regions. Incorporat-

ing the auxiliary objective yields improved calibration.

Comparison of PCP Score and Absolute Residue Score. Table 2 compares the average calibration score and average prediction interval width between CP-Traj, which uses the PCP score, and CP-Traj with the absolute residue score. The absolute residue score, defined as $s(y, \hat{y}) = |y - \hat{y}|$, with \hat{y} taken as the mean of all samples, is one of the most commonly used non-conformity scores for regression problems. However, it is not designed for sampled trajectories and thus cannot construct prediction intervals around each sample, failing to capture the inherent temporal dependencies. From Table 2, we see that using the PCP score in our method consistently provides better coverage and generally improves efficiency.

Conclusion

We are among the first to introduce CP-Traj for calibrating sampled trajectories in an online setting. Our framework incorporates a novel online update step that produces a set of values, each guaranteeing long-term coverage. This update step enables further optimization across the forecast horizon. By combining the PCP score with this optimization, CP-Traj handles diverging trajectories and inter-step dependencies. Experiments on multiple real-world datasets and one synthetic dataset demonstrate that our method yields sharper prediction intervals with improved coverage, highlighting the effectiveness of our approach.

Limitations and Future Work: Our method has several limitations. First, while it provides a long-term coverage guarantee, our experiments indicate that the convergence rate is sensitive to the choice of parameters and objective functions. If these are not selected appropriately, the initial calibration performance may be suboptimal. Second, our approach does not include a mechanism for sample rejection. As a result, when many samples are of poor quality, the efficiency of the intervals may be reduced. Future work can explore methods like adopting multiple experts with different parameters to avoid parameter selection and achieve better adaptivity. And explore sample rejection methods to improve the efficiency of the prediction intervals.

Acknowledgements

This work was supported in part by the Centers for Disease Control and Prevention Award NU38FT000002 and start-up funds from the University of Michigan. We gratefully acknowledge Professor Xianglei Huang for his valuable assistance with the Cyclone dataset used in this study.

References

- Angelopoulos, A.; Candes, E.; and Tibshirani, R. J. 2023. Conformal pid control for time series prediction. *Advances in neural information processing systems*, 36: 23047–23074.
- Barber, R. F.; Candes, E. J.; Ramdas, A.; and Tibshirani, R. J. 2023. Conformal prediction beyond exchangeability. *The Annals of Statistics*, 51(2): 816–845.
- Bhatnagar, A.; Wang, H.; Xiong, C.; and Bai, Y. 2023. Improved online conformal prediction via strongly adaptive online learning. In *International Conference on Machine Learning*, 2337–2363. PMLR.
- Cachay, S. R.; Aittala, M.; Kreis, K.; Brenowitz, N.; Vahdat, A.; Mardani, M.; and Yu, R. 2025. Elucidated Rolling Diffusion Models for Probabilistic Weather Forecasting. *arXiv preprint arXiv:2506.20024*.
- Chandra, R.; and He, Y. 2021. Bayesian neural networks for stock price forecasting before and during COVID-19 pandemic. *Plos one*, 16(7): e0253217.
- Chang, M.-F.; Lambert, J. W.; Sangkloy, P.; Singh, J.; Bak, S.; Hartnett, A.; Wang, D.; Carr, P.; Lucey, S.; Ramanan, D.; and Hays, J. 2019. Argoverse: 3D Tracking and Forecasting with Rich Maps. In *Conference on Computer Vision and Pattern Recognition (CVPR)*.
- Cramer, E. Y.; Ray, E. L.; Lopez, V. K.; Bracher, J.; Brennen, A.; Castro Rivadeneira, A. J.; Gerding, A.; Gneiting, T.; House, K. H.; Huang, Y.; et al. 2022. Evaluation of individual and ensemble probabilistic forecasts of COVID-19 mortality in the United States. *Proceedings of the National Academy of Sciences*, 119(15): e2113561119.
- Ding, Y.; Park, Y.; Gopalswamy, K.; Hasson, H.; Wang, Y. B.; and Huan, L. 2023. Dynamic ensemble for probabilistic time-series forecasting via deep reinforcement learning.
- Feng, S.; Miao, C.; Zhang, Z.; and Zhao, P. 2024. Latent diffusion transformer for probabilistic time series forecasting. In *Proceedings of the AAAI Conference on Artificial Intelligence*, volume 38, 11979–11987.
- Frazier, P. I. 2018. A tutorial on Bayesian optimization. *arXiv preprint arXiv:1807.02811*.
- Gibbs, I.; and Candes, E. 2021. Adaptive conformal inference under distribution shift. *Advances in Neural Information Processing Systems*, 34: 1660–1672.
- Gibbs, I.; and Candès, E. J. 2024. Conformal inference for online prediction with arbitrary distribution shifts. *Journal of Machine Learning Research*, 25(162): 1–36.
- Jospin, L. V.; Laga, H.; Boussaid, F.; Buntine, W.; and Benamoun, M. 2022. Hands-on Bayesian neural networks—A tutorial for deep learning users. *IEEE Computational Intelligence Magazine*, 17(2): 29–48.
- Kamarthi, H.; Kong, L.; Rodríguez, A.; Zhang, C.; and Prakash, B. A. 2021. When in Doubt: Neural Non-Parametric Uncertainty Quantification for Epidemic Forecasting. *Advances in Neural Information Processing Systems*, 34.
- Koenker, R.; and Hallock, K. F. 2001. Quantile regression. *Journal of economic perspectives*, 15(4): 143–156.
- Kuleshov, V.; Fenner, N.; and Ermon, S. 2018. Accurate uncertainties for deep learning using calibrated regression. In *International conference on machine learning*, 2796–2804. PMLR.
- Lakshminarayanan, B.; Pritzel, A.; and Blundell, C. 2017. Simple and scalable predictive uncertainty estimation using deep ensembles. *Advances in neural information processing systems*, 30.
- Li, R.; and Rodríguez, A. 2025. Neural Conformal Control for Time Series Forecasting. In *Proceedings of the AAAI Conference on Artificial Intelligence*, volume 39, 18439–18447.
- Liang, F. 2005. Bayesian neural networks for nonlinear time series forecasting. *Statistics and computing*, 15(1): 13–29.
- Lim, B.; Arık, S. Ö.; Loeff, N.; and Pfister, T. 2021. Temporal fusion transformers for interpretable multi-horizon time series forecasting. *International journal of forecasting*, 37(4): 1748–1764.
- MacKay, D. J. 1992. A practical Bayesian framework for backpropagation networks. *Neural computation*, 4(3): 448–472.
- Mathis, S. M.; Webber, A. E.; León, T. M.; Murray, E. L.; Sun, M.; White, L. A.; Brooks, L. C.; Green, A.; Hu, A. J.; Rosenfeld, R.; et al. 2024. Evaluation of FluSight influenza forecasting in the 2021–22 and 2022–23 seasons with a new target laboratory-confirmed influenza hospitalizations. *Nature communications*, 15(1): 6289.
- Ouyang, Y.; and Yin, H. 2018. Multi-step time series forecasting with an ensemble of varied length mixture models. *International journal of neural systems*, 28(04): 1750053.
- Rasul, K.; Seward, C.; Schuster, I.; and Vollgraf, R. 2021. Autoregressive denoising diffusion models for multivariate probabilistic time series forecasting. In *International conference on machine learning*, 8857–8868. PMLR.
- Rodríguez, A.; Kamarthi, H.; Agarwal, P.; Ho, J.; Patel, M.; Sapre, S.; and Prakash, B. A. 2024. Machine learning for data-centric epidemic forecasting. *Nature Machine Intelligence*, 6(10): 1122–1131.
- Shen, L.; and Kwok, J. 2023. Non-autoregressive conditional diffusion models for time series prediction. In *International Conference on Machine Learning*, 31016–31029. PMLR.
- Tibshirani, R. J.; Foygel Barber, R.; Candes, E.; and Ramdas, A. 2019. Conformal prediction under covariate shift. *Advances in neural information processing systems*, 32.
- Ullrich, P. A.; and Zarzycki, C. M. 2017. TempestExtremes: a framework for scale-insensitive pointwise feature tracking on unstructured grids. *Geoscientific Model Development*, 10(3): 1069–1090.

- Ullrich, P. A.; Zarzycki, C. M.; McClenny, E. E.; Pinheiro, M. C.; Stansfield, A. M.; and Reed, K. A. 2021. TempestExtremes v2.1: a community framework for feature detection, tracking, and analysis in large datasets. *Geoscientific Model Development*, 14(8): 5023–5048.
- Vovk, V. 2012. Conditional validity of inductive conformal predictors. In *Asian conference on machine learning*, 475–490. PMLR.
- Vovk, V.; Gammerman, A.; and Shafer, G. 2005. *Algorithmic learning in a random world*. Springer.
- Vuletić, M.; Prenzel, F.; and Cucuringu, M. 2024. Fin-gan: Forecasting and classifying financial time series via generative adversarial networks. *Quantitative Finance*, 24(2): 175–199.
- Wang, Z.; Gao, R.; Yin, M.; Zhou, M.; and Blei, D. 2023. Probabilistic Conformal Prediction Using Conditional Random Samples. 8814–8836.
- Xu, C.; and Xie, Y. 2021. Conformal prediction interval for dynamic time-series. In *International Conference on Machine Learning*, 11559–11569. PMLR.
- Yalavarthi, V. K.; Scholz, R.; Born, S.; and Schmidt-Thieme, L. 2025. Probabilistic Forecasting of Irregularly Sampled Time Series with Missing Values via Conditional Normalizing Flows. In *Proceedings of the AAAI Conference on Artificial Intelligence*, volume 39, 21877–21885.
- Yang, Z.; Candès, E.; and Lei, L. 2024. Bellman conformal inference: Calibrating prediction intervals for time series. *arXiv preprint arXiv:2402.05203*.
- Yoon, J.; Jarrett, D.; and Van der Schaar, M. 2019. Time-series generative adversarial networks. *Advances in neural information processing systems*, 32.
- Zaffran, M.; Féron, O.; Goude, Y.; Josse, J.; and Dieuleveut, A. 2022. Adaptive conformal predictions for time series. In *International Conference on Machine Learning*, 25834–25866. PMLR.
- Zarzycki, C. M.; and Ullrich, P. A. 2017. Assessing sensitivities in algorithmic detection of tropical cyclones in climate data. *Geophysical Research Letters*, 44(2): 1141–1149.
- Zecchin, M.; Park, S.; and Simeone, O. 2024. Forking uncertainties: Reliable prediction and model predictive control with sequence models via conformal risk control. *IEEE Journal on Selected Areas in Information Theory*, 5: 44–61.

Related Works

Uncertainty Quantification for Time Series

Time series forecasting involves using historical observations to predict future values. The uncertainty in these predictions can arise from multiple sources, including the intrinsic stochasticity of the data-generating process, the quantity and quality of observed data, and the limitations of the forecasting models themselves. Quantifying uncertainty in time series forecasting is essential, especially given its widespread use in practical applications. Understanding the variability and potential range of predictions is particularly important in high-stakes domains such as stock price forecasting and public health. A number of time series uncertainty quantification methods have been developed. Ensemble-based methods (Lakshminarayanan, Pritzel, and Blundell 2017; Ding et al. 2023) are among the most widely used approaches for uncertainty quantification, aggregating predictions from multiple individual models to estimate uncertainty. However, these methods often incur significantly higher computational costs, as they require running multiple models concurrently. Bayesian methods (MacKay 1992; Liang 2005; Chandra and He 2021) can be regarded as a form of ensemble-based approach, where a distribution over model parameters is learned. Based on this distribution, Bayesian methods produce a predictive distribution over the target variable (Josquin et al. 2022). However, these methods can become computationally expensive as the number of parameters grows. Moreover, their performance is sensitive to the assumptions made about the underlying distribution; incorrect assumptions can adversely affect predictive accuracy. Other widely used methods for uncertainty quantification in time series forecasting include diffusion models (Rasul et al. 2021), quantile regression (Koenker and Hallock 2001), and related approaches.

Conformal Prediction

Conformal prediction is a framework specifically developed for uncertainty quantification. Originally, it was introduced as a distribution-free method for i.i.d. data, providing finite-sample coverage guarantees under the exchangeability assumption (Vovk, Gammerman, and Shafer 2005; Vovk 2012). Unlike the aforementioned methods, conformal prediction does not require distributional assumptions, making it a robust approach for uncertainty quantification. However, in practice, the exchangeability assumption is often violated due to factors such as distribution shifts and temporal dependencies. To address these challenges, many methods have been developed to extend the conformal prediction framework to non-exchangeable settings (Tibshirani et al. 2019; Xu and Xie 2021; Barber et al. 2023; Gibbs and Candès 2021).

Online Conformal Prediction

ACI (Gibbs and Candès 2021) is one of the methods that is specifically designed for online scenarios, where data arrive sequentially and the forecasting model is continuously updated. ACI provides a long-term coverage guarantee, ensuring that the empirical coverage rate converges to the user-

specified level as time progresses, without relying on any distributional assumptions. One line of work, known as conformal control, can be viewed as a variant of ACI (Yang, Candès, and Lei 2024). These methods adopt similar update steps as ACI to achieve theoretical long-term coverage guarantees. For example, Conformal PID (Angelopoulos, Candès, and Tibshirani 2023) replaces ACI’s update step with a more adaptive PID controller to improve adaptivity. AgACI (Zaffran et al. 2022) examines the impact of different learning rates and employs an online expert aggregation technique to eliminate the need for manual tuning. Similarly, FACI (Gibbs and Candès 2024) is a parameter-free version of ACI that adapts learning rates over time to achieve provably lower regret. Despite these advances, multi-step online conformal prediction remains an underexplored area.

Theory

Theorem 1. *For any horizon h , when $\delta_t = o(t)$, applying the update step in Algorithm 1 produces a range of calibration threshold values I_t^h at each time step t . For any $\alpha^{h*} \in I_t^h$, the procedure guarantees long-term coverage.*

Now we show a proof for Theorem 1 following ACI (Gibbs and Candès 2021). First we simplify the notation here as we only consider one horizon h without loss of generality. The update step at time t can be written as

$$(1) \quad \text{err}_t = \mathbf{1}\{y_t \notin C_t\}, \quad (9)$$

$$(2) \quad \alpha_{t+1} = \alpha_t + \eta(\alpha - \text{err}_t), \quad (10)$$

$$(3) \quad \alpha_{t+1}^* \in [\alpha_{t+1} - \delta_{t+1}, \alpha_{t+1} + \delta_{t+1}]. \quad (11)$$

Lemma 2 (Boundedness of α_t).

$$\forall t, \alpha_{t+1} \in [-\eta - \delta_t, 1 + \eta + \delta_t].$$

Proof. First of all, from the update rule, we have:

$$|\alpha_{t+1} - \alpha_t| = \eta|\alpha - \text{err}_t| \leq \eta.$$

Assume, for the sake of contradiction, that there exists a time t such that $\alpha_{t+1} < -\eta - \delta_t$. Therefore, there must exist some t where $\alpha_t < -\delta_t$ and $\alpha_{t+1} < \alpha_t$. However, when $\alpha_t < -\delta_t$, it follows that $\alpha_t^* < 0$. Then $\hat{Q}_t(1 - \alpha_t^*) = \infty$, which implies $\text{err}_t = 0$. Substituting into the update rule gives:

$$\alpha_{t+1} = \alpha_t + \eta(\alpha - 0) = \alpha_t + \eta\alpha \geq \alpha_t,$$

which contradicts the assumption that $\alpha_{t+1} < \alpha_t$.

An analogous argument applies for the case $\alpha_{t+1} > 1 + \eta + \delta_t$. \square

Proof of Theorem 1. Using the update rule $\alpha_{t+1} - \alpha_t = \eta(\alpha - \text{err}_t)$, sum from $t = 1$ to $t = T$ to get a telescoping series:

$$\alpha_{T+1} = \alpha_1 + \eta \sum_{t=1}^T (\alpha - \text{err}_t)$$

According to the boundedness of α_{T+1} ,

$$\alpha_1 + \eta \sum_{t=1}^T (\alpha - \text{err}_t) \in [-\eta - \delta_T, 1 + \eta + \delta_T]$$

Rearranging and divided by η yields:

$$\frac{1}{T} \sum_{t=1}^T (\alpha - \text{err}_t) \leq \frac{\max\{\alpha, 1 - \alpha\} + \eta + \delta_T}{T\eta}$$

When $\delta_t = o(t)$, we have

$$\frac{\max\{\alpha, 1 - \alpha\} + \eta + \delta_T}{T\eta} = o(1),$$

which converges to zero as $T \rightarrow \infty$. \square

More on the Method

Customization of F : The optimization step relies on the distribution $F_t^h = \{\beta_{t-h}^h, \dots, \beta_{t-B}^h\}$ to approximate the ground truth value y_t^h . Consequently, the quality of F_t^h significantly influences the effectiveness of selecting the optimal calibration threshold α^* during optimization. In addition, the set F_t^h can be customized to serve different purposes. For instance, when the user prioritizes worst-case performance or when distributional shifts cause F_t^h to deviate substantially from the true distribution, it may be preferable to restrict the set to a subset of values. To this end, we introduce a parameter θ that acts as a quantile threshold. We define the trimmed set $F_t^h(\theta)$ as containing only those values in F_t^h that are below the θ -th quantile.

Experiments

More Details on the Datasets and Base Forecasters.

We compare our approach using both synthetic and publicly available real-world datasets across applications in autonomous navigation, climate forecasting, and healthcare. The *Argoverse*³ autonomous vehicle dataset provides birds-eye-view 2D centroids of vehicles in urban traffic scenarios, sampled at 10 Hz in Miami and Pittsburgh (Chang et al. 2019). The training set contains 29,201 sequences, while the test set consists of 4,774 sequences. We adopt the K-NN Regressor from the official Argoverse baselines and adapt it for online prediction, using an observation window of 10 steps and a prediction horizon of 5 steps, generating 9 predicted trajectories per iteration. We use 250 sequences. The Cyclone dataset is constructed based on data from Weather Lab⁴ (Ullrich and Zarzycki 2017; Zarzycki and Ullrich 2017; Ullrich et al. 2021), a research platform developed by Google DeepMind and Google Research that shares AI-based stochastic neural network models for cyclone prediction. Weather Lab is capable of forecasting cyclone trajectories up to 15 days in advance with a temporal resolution of 6 hours. We downloaded both the observational data and experimental model predictions provided by Google. Our experiments consider 30 historical cyclone scenarios, each spanning at least 4 days, with 5 predicted trajectories generated over an 8-step horizon for each scenario. The synthetic dataset, Markovar, is generated using a Markovian Auto-Regressive (MarkovAR) process, which

allows us to evaluate our approach under controlled conditions. The underlying system evolves based on a transition matrix, with each state having a 98% probability of remaining unchanged at each step. At every time step t , the process produces an observation based on the current latent state using an AR(1) model. For predicted trajectories, at each step, the simulation model, which uses the same model as the underlying model, randomly generates 16 predicted trajectories over a 32-step horizon, repeating this process sequentially. We generate three sequences, each with 500 observations, for the experiments.

The final dataset, Flusight, is constructed from data published by the CDC’s FluSight forecasting initiative⁵ (Mathis et al. 2024), which contains publicly available records of influenza hospitalizations. Following prior work in this area (Rodríguez et al. 2024), we adopt a weekly online prediction setting. We utilize observations and model predictions from multiple teams (excluding FluSight ensemble models) during the 2023–2024 and 2024–2025 respiratory seasons, retaining only those weeks where at least 10 teams submitted predictions. This datasets use 50 sequences from different locations in the United States. Three locations’ data is excluded due to insufficient data. The total weeks for each sequence in this dataset is around 50 weeks. In this setting, the model generates 5 predicted trajectories over an 4-step horizon for evaluation.

Experimental Setup

All experiments are conducted on a Linux system. Each dataset-method combination requires approximately 30 seconds to 2 minutes to complete. The code is included in the supplementary material.

Hyperparameters for each method are provided in the `configs/` directory of the codebase. These parameters are tuned on the Lane dataset, using 250 sequences apart from those used for evaluation. We employed a Bayesian hyperparameter tuning framework (Frazier 2018) to optimize several parameters, including the learning rate (η), which controls the update speed of the calibration threshold based on coverage errors; the number of β values in the empirical distribution F (B); the learning rate for horizon coverage calibration threshold updates; and the threshold for selecting β values in F . The tuning process consisted of 100 iterations, taking roughly 5 hours in total. For the other datasets, we generally applied similar hyperparameter settings without further tuning.

Evaluation

We mainly use calibration score (Kuleshov, Fenner, and Ermon 2018) and interval width as the evaluation metrics. Below are the details on how they are computed.

Given the coverage condition for each time step, each mis-coverage rate α_i and each horizon h , denote the coverage condition as $\text{cov}_t^h(\alpha_i)$, which equals to 1 if the ground truth is covered, otherwise 0.

Calibration Score: To compute the calibration score for one horizon h , first compute the average coverage for each α :

³<https://github.com/jagjeet-singh/argoverse-forecasting>

⁴<https://deepmind.google.com/science/weatherlab>

⁵<https://github.com/cdcepi/FluSight-forecast-hub>

$\text{cov}^h(\alpha_i) = \frac{1}{T} \sum_{t=1}^T \text{cov}_t^h(\alpha_i)$. Then the calibration score for one horizon h is

$$\frac{1}{N} \sum_{i=1}^N |\text{cov}^h(\alpha_i) - (1 - \alpha_i)|.$$

The average calibration score is averaged over each horizon and all sequences.

Interval Width: For the one-dimensional datasets Marko-var and Flusight, the interval width is calculated as the total length of the merged prediction intervals formed around each sample. In contrast, for the two-dimensional datasets Lane and Cyclone, the interval width corresponds to the total area covered by the prediction sets.

An Example of User-Specified Objective Function: Increasing Uncertainty

One of the advantage of our method is that it allows optimizing for user-specified objectives. Here we provide an example. In time series forecasting, due to temporal dependencies, the uncertainty generally accumulates over the forecast horizons (Ouyang and Yin 2018; Cachay et al. 2025). Thus, a reasonable objective is to encourage the prediction interval to expand over forecast steps.

$$J_{inc} = \min \sum_{h=2}^H \max(0, \lambda_J u_h - u_{h-1}),$$

where $\lambda_J \in [0, \infty)$ is a parameter that controls the strictness of the objective. When $\lambda_J = 0$, J_{inc} has no effect. As λ_J increases, the optimization increasingly enforces that the prediction interval at horizon h is larger than that at $h - 1$ to avoid penalty.